ELSEVIER

Microporous and Mesoporous Materials 50 (2001) 209–218

MICROPOROUS AND MESOPOROUS MATERIALS

www.elsevier.com/locate/micromeso

Redox behavior and selective oxidation properties of mesoporous titano- and zirconosilicate MCM-41 molecular sieves

K. Chaudhari, R. Bal, D. Srinivas *, A.J. Chandwadkar, S. Sivasanker

Catalysis Division, National Chemical Laboratory, Pune 411008, India

Received 21 March 2001; received in revised form 8 August 2001; accepted 28 September 2001

Abstract

Mesoporous titano- and zirconosilicate molecular sieves, Ti-MCM-41 and Zr-MCM-41, respectively, with Si/M ratios in the range from 11 to 96 (M = Ti or Zr), have been synthesized by the hydrothermal method and characterized by XRD, XRF, N_2 adsorption and diffusive reflectance UV–Vis (DRUV–Vis), FT-IR and electron spin resonance (ESR) spectroscopic techniques. The redox behavior and selective oxidation properties of these materials have been investigated. ESR of samples reduced with $LiAlH_4$ (298 K) and H_2 (673–873 K) reveals two types of metal ion species: species I′ located inside the pore walls and species I″ located at the pore surface. The reduced species I″ are highly reactive towards oxygen and form $M(O_2^{-\cdot})$ radicals. The $M(O_2^{-\cdot})$ radicals were also observed when the samples were reacted with aqueous H_2O_2 or *tert*-butylhydroperoxide (TBHP). ESR studies reveal that Ti-MCM-41 is easier to reduce and reoxidize than Zr-MCM-41. The DRUV–Vis spectra are consistent with a monoatomic dispersion of the metal ions. In the samples with high metal loading the presence of a nanocrystalline metal oxide phase cannot be ruled out. Both Ti-MCM-41 and Zr-MCM-41 catalyze the hydroxylation of 1-naphthol with aqueous H_2O_2 and the epoxidation of norbornylene with TBHP. © 2001 Elsevier Science B.V. All rights reserved.

Keywords: Mesoporous molecular sieves; MCM-41; Titanosilicates; Zirconosilicates; Electron spin resonance; Hydroxylation of 1-naphthol; Epoxidation of norbornylene

---

1. Introduction

Metallosilicate molecular sieves, obtained by isomorphous substitution of Si by metal ions in silicate structures, exhibit catalytic activity in selective oxidation reactions using hydrogen peroxide and alkylhydroperoxides at mild conditions. Among the microporous metallosilicates, titanium-substituted silicalite-1 (TS-1; MFI topology; pore diameter ~ 5.5 Å) is unique in catalyzing a variety of selective oxidation reactions [1,2]. In recent years, attention has increasingly been directed towards the study of metal-containing mesoporous M41S type molecular sieves with large pores (20–100 Å diameter) suitable for the transformation of bulky organic compounds [3–8]. Metal ions such as Al [9–12], Ti [13,14], Fe [15], Mn [16], V [17,18], and Ga [19–21] have been successfully incorporated into the MCM-41 framework. The catalytic

---

* Corresponding author. Tel.: +91-020-589-3300; fax: +91-020-589-3761.

E-mail address: srinivas@cata.ncl.res.in (D. Srinivas).

1387-1811/01/$ - see front matter

PII: S1387-1811(01)00454-1

activity of these modified MCM-41 materials has been examined in the selective oxidation of substrates such as hex-1-ene, α-terpineol, norbornylene and 2,6-di-*tert*-butylphenol. Titanium- and zirconium-containing MCM-41 materials have been reported to be useful as catalysts and catalyst supports [22–25]. Kevan and co-workers [26–28] reported on the electron spin resonance (ESR) spectroscopic characterization of Ti-MCM-41 samples irradiated with γ-rays. Recently, we have reported detailed spectroscopic investigations on the incorporation of Sn(IV) [29] and Zr(IV) [30] ions in MCM-41. The present study deals with the redox behavior and catalytic activity of mesoporous titano- and zirconosilicate molecular sieves (Ti-MCM-41 and Zr-MCM-41) with varying metal contents (Si/M = 11–96) prepared by hydrothermal methods. Characterization of the samples by XRD, XRF, N_2 adsorption, FT-IR, diffuse reflectance UV–Visible (DRUV–Vis) and ESR prove the substitution of metal ions in the framework of the MCM-41 structure.

2. Experimental

2.1. Materials

The MCM-41 samples were synthesized hydrothermally, using fumed silica (99%, Sigma), tetramethylammonium silicate (TMA silicate; 10 wt.% silica solution, $TMA/SiO_2 = 0.5$; Sachem Inc., USA), cetyltrimethylammonium chloride/hydroxide (CTMACl/OH; 17.9 wt.% Cl and 6.7 wt.% OH) prepared in the laboratory by partial exchange of CTMACl (25 wt.% aqueous solution, Aldrich) over an ion exchange resin, TMA hydroxide (TMAOH; 99%, Aldrich) and titanium butoxide and zirconium butoxide (80 wt.% solution in 1-butanol, Aldrich). The all-silica MCM-41 (Si-MCM-41) and Zr-MCM-41 samples were prepared as reported earlier [30].

2.2. Synthesis of Ti-MCM-41

The molar composition of the synthesis gel of Ti-MCM-41, in terms of oxides, was as follows:

$$SiO_2 : 0\text{–}0.08\ TiO_2 : 0.089\ (CTMA)_2O : 0.155\ (TMA)_2O : 18H_2O.$$

In a typical synthesis (Ti-MCM-41(B)), a 24.6% solution of CTMACl/OH (16.7 g) was placed in a polypropylene beaker, and 2.08 g TMAOH dissolved in 10 g water and 13.6 g TMA silicate were added to it while stirring. The thick gel formed was stirred for 15 min. Fumed silica (3.1 g) was then added slowly in about 10 min to the above mixture under stirring. After complete addition the stirring was continued for 1 h. To this thick slurry, 0.52 g of $Ti(OC_4H_9)_4$ (for Si/Ti = 50) in 5–6 g of isopropanol were added. Stirring was continued for another 1 h. The pH of the final slurry was maintained at 11.5 using 0.1 N H_2SO_4. The mixture was then transferred to a stainless steel autoclave and heated at 383 K for 5 days. The solid material (Ti-MCM-41(B)) was filtered, washed with deionized water and dried at 373 K in air. The product was then calcined at 823 K, first in flowing nitrogen (for 3 h) and then in flowing air (for 6 h) to remove the organic matter.

Three Ti-MCM-41 and four Zr-MCM-41 samples with different metal contents were synthesized. The synthesis of these materials is reproducible. The compositions of the gels and calcined solids and their physicochemical characteristics are presented in Table 1. All the Zr-containing samples and Si-MCM-41 were reported earlier [30], and the data for these materials are included in Table 1 for completeness.

Ti- and Zr-impregnated MCM-41 samples (Ti-MCM-41(Imp) and Zr-MCM-41(Imp), respectively) with Si/M ratios of 25 were prepared by adding 0.26 g of $Ti(OC_4H_9)_4$ and 0.35 g of $Zr(OC_4H_9)_4$, respectively, dissolved in 5 g of 2-propanol to 1 g of dry Si-MCM-41. The mixture was gently heated to dryness while stirring. The samples were finally calcined at 573 K in flowing air for 4 h.

2.3. Physicochemical characterization

X-ray diffractograms of the calcined samples were recorded on a Rigaku Miniflex diffractometer using nickel-filtered CuKα radiation ($\lambda =$

Table 1
Composition and physicochemical characteristics of Ti-MCM-41 and Zr-MCM-41 samples

Sample	SiO_2/MO_2 (mole ratio)		XRD d_{100} (Å)	BET surface area (m^2/g)	Pore diameter (Å)	Pore volume (cm^3/g)
	Gel	Product				
Si-MCM-41	–	–	36.77	975	27	0.63
Ti-MCM-41(A)	100	63	39.75	–	–	–
Ti-MCM-41(B)	50	34	40.92	963	30	0.90
Ti-MCM-41(C)	25	18	41.64	914	32	0.98
Zr-MCM-41(A)	100	96	38.38	968	28	0.75
Zr-MCM-41(B)	50	55	39.76	942	30	0.90
Zr-MCM-41(C)	25	39	40.88	889	31	1.05
Zr-MCM-41(D)	12.5	23	33.69	766	25	0.51

1.5406 Å, 30 kV, 15 mA) over $2\theta = 1.5$–$10°$ and a scan speed of 1°/min. The chemical composition was determined using a Rigaku 3070 E wavelength dispersive XRF spectrometer with a Rh target energized at 50 kV and 40 mA. The surface area and pore diameter of the samples were determined from N_2 adsorption isotherms (obtained on a Coulter 100 instrument), using the Barret–Joyner–Halenda (BJH) model [31]. DRUV–Vis spectra of the solid samples were recorded on a Shimadzu UV-2101 PC spectrophotometer. FT-IR spectra of the samples as KBr pellets were taken on a Pye Unicam SP-300 spectrophotometer.

ESR spectra were recorded on a Bruker EMX spectrometer operating at X-band frequency and 100 kHz field modulation. The spectra at 77 K were measured using a quartz finger dewar. Spectral simulations were performed using the Bruker Simfonia software package. ESR experiments were carried out on the samples reacted with dry hydrogen or $LiAlH_4$. Prior to the reduction with dry hydrogen, the samples were evacuated (10^{-1} Pa) and dehydrated by gradually raising the temperature from 298 K to a set value (673, 773 or 883 K) in about 4–5 h and then kept at that temperature for a further period of 6 h. The samples, thus activated, were treated with a flow of dry hydrogen (20 cm^3/min) at the set temperature for 6 h. Then the samples were cooled to 298 K and transferred into ESR tubes. Reduction with $LiAlH_4$ in anhydrous distilled THF was carried out under argon atmosphere at 298 K for 6 h.

ESR measurements were also done on samples reacted with 25% aqueous H_2O_2 or *tert*-butylhydroperoxide (TBHP) (70% aqueous solution, Aldrich). In those cases the catalysts (45 mg) were initially activated at 673 K, and then 0.1 cm^3 of oxidant solution were added at 298 K till the sample became wet.

2.4. Catalytic activity

Catalytic activities of the samples in the hydroxylation of 1-naphthol and epoxidation of norbornylene were studied using a batch reactor at atmospheric pressure. Aqueous H_2O_2 was used as oxidant in the hydroxylation of 1-naphthol and TBHP in the epoxidation of norbornylene.

In a typical reaction, 0.5 g of substrate (1-naphthol or norbornylene), 10 g of CH_3CN and 0.1 g of solid catalyst were taken in a 50 cm^3 round-bottom flask with a water-cooled condenser. The reactions were conducted at 353 K in the oxidation of 1-naphthol and at 343 K in the expoxidation of norbornylene. An optimum amount of oxidant (substrate/oxidant (mole ratio) = 1.5) was added to the reaction mixture, and the reaction was carried out for 24 h. The products were analyzed by a GC (HP-5880 A) equipped with a methyl silicon gum capillary column (HP1, 50 m long and 0.2 mm i.d.) and a flame ionization detector.

3. Results and discussion

3.1. Material characterization

3.1.1. XRD

The XRD patterns of the as-synthesized Ti-MCM-41 and Zr-MCM-41 samples resembled

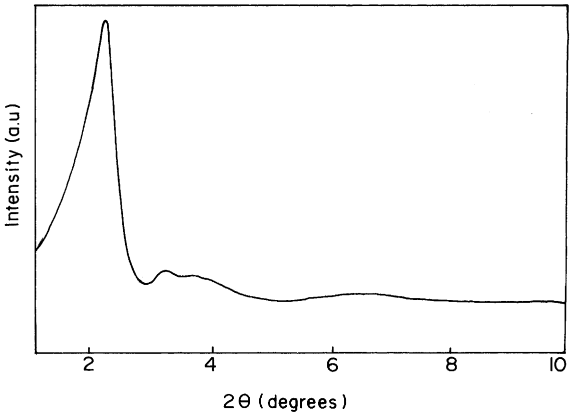

Fig. 1. Powder XRD pattern of calcined Ti-MCM-41(B).

those of Si-MCM-41 [3,4]. The long-range order in hexagonal symmetry was retained in the calcined forms of silicious and metal-incorporated MCM-41 samples. A typical XRD profile of calcined Ti-MCM-41 is shown in Fig. 1, and the d_{100} values for all the samples are listed in Table 1. The XRD peaks shift to higher *d*-values with increasing metal content consistent with a probable incorporation of Ti and Zr into the MCM-41 structure.

3.1.2. Sorption

All samples exhibited type IV isotherms typical of a mesoporous texture. The BET surface area, pore size and pore volume calculated by using the BJH model [31] are listed in Table 1. In general, the pore diameter and pore volume of the samples increased while the surface area decreased with increasing metal content.

3.1.3. FT-IR and DRUV–Vis spectroscopy

Ti-MCM-41 and Zr-MCM-41 exhibited a band at 964 and 960 cm^{-1}, respectively, in the FT-IR spectra (KBr pellets) attributable to the Si–O–(M) group of the framework. However, caution is required in assigning this band, as Si-MCM-41 samples also exhibit such a band around 960 cm^{-1} due to silanol groups at the defect sites. DRUV–Vis spectra of Ti-MCM-41 and Zr-MCM-41 samples showed a band, due to oxygen to metal charge transfer transition, at 220 and 208 nm, respectively (Fig. 2). In calcined samples, this band shifted to the lower energy side by about 5 nm. The difference in band position for Ti- and Zr-MCM-41 samples is due to the difference in electronegativity of the metal ion and covalency of the metal–oxygen bond. The Ti–O bond is more covalent than the Zr–O bond. TiO_2 (anatase) showed this band at around 340 nm (Fig. 2) and ZrO_2 at 240 nm. The shift in the charge transfer band position towards the higher energy side in Ti-MCM-41 and Zr-MCM-41 compared to pure TiO_2 (anatase) and ZrO_2, respectively, indicates monoatomic dispersion and tetrahedral coordination of Ti and Zr in the MCM-41 structure. A similar shift in the charge transfer band position was reported earlier for other metallosilicates [1,2,7–15].

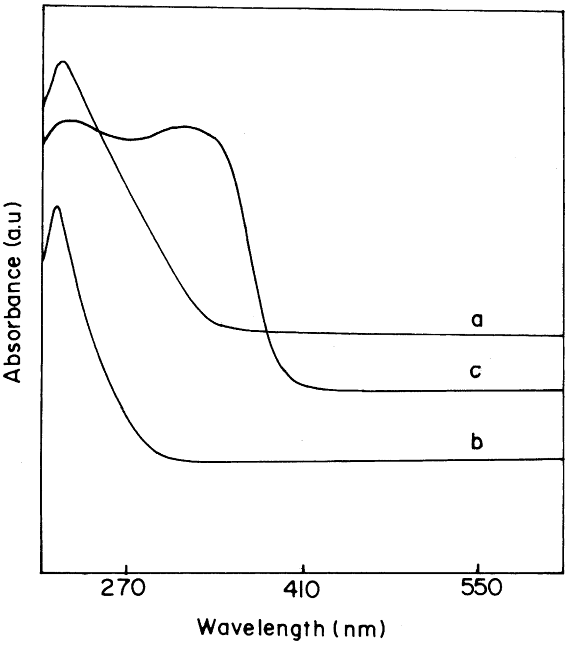

Fig. 2. DRUV–Vis spectra of calcined samples after smoothening: (a) Ti-MCM-41(B), (b) Zr-MCM-41(B) and (c) TiO_2 (anatase).

3.1.4. ESR spectroscopy

Both Ti-MCM-41 and Zr-MCM-41 were ESR silent consistent with the +4 oxidation state of Ti and Zr ions in the MCM-41 structure. On reaction with dry hydrogen the samples became paramagnetic and showed two sets of ESR signals, with one set of signals having *g* values below the free-spin g-value ($g_e = 2.0023$) and the other set of signals above the free-spin g-value. The intensity of the signals increased with increasing metal content. The all-silica sample (Si-MCM-41) treated with dry hydrogen did not show these signals indicating the origin of the ESR signals as due to the incorporated metal ions. The signals with g-values below the free-spin value are typical of Ti(III) and Zr(III) ions, while the signals occurring above the free-spin g-value are due to metal superoxide radical species, $M(O_2^{-\cdot})$ [30,32]. The intensities of Ti(III) signals as in the case of Zr(III) [30] were higher in samples reduced at 873 K. Typical ESR spectra of hydrogen-reduced Ti-MCM-41 with varying Si/Ti ratio are shown in Fig. 3. Related spectra for Zr-MCM-41 samples were reported earlier [30]. The overall spectral intensity is higher for Ti-MCM-41 than for Zr-MCM-41 and suggests that Ti(IV) ions are easier to reduce than Zr(IV) ions. This is in agreement with the difference in the charge transfer band positions of the Ti-MCM-41 and Zr-MCM-41 samples in the DRUV–Vis spectra (the former showed the charge transfer band at a lower energy than the latter). The stability of Ti(III) ions was examined by exposing the samples to aerial oxygen. As shown in Fig. 4, the dominant signal of the air-exposed samples was due to metal superoxide species. In other words Ti(III) is highly reactive towards aerial oxygen to form metal superoxide radicals. Weak Ti(III) signals present even after 16 h of air exposure indicate that a small fraction of the Ti ions are located deep inside the pore walls not accessible for re-oxidation with aerial oxygen, while the majority of the Ti ions are near the pore surface.

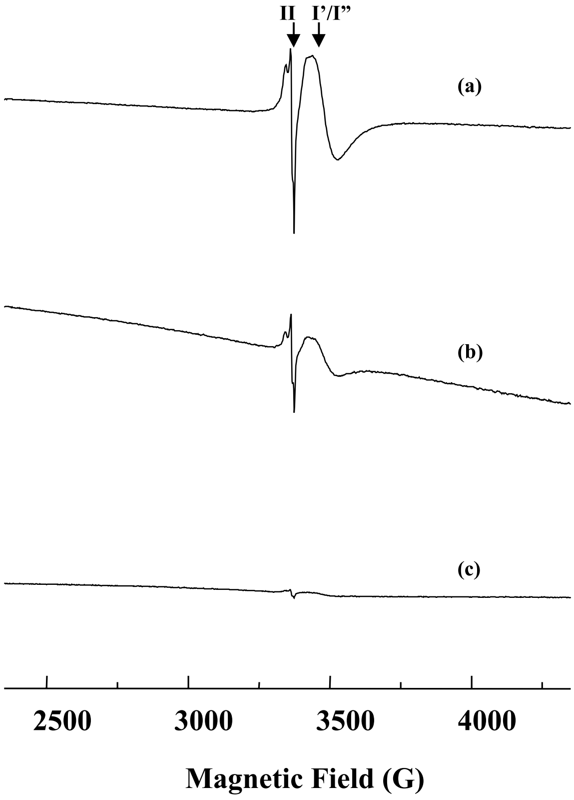

Fig. 3. ESR spectra (at 77 K) of Ti-MCM-41 reduced at 873 K: (a) sample C, (b) sample B and (c) sample A. Signals due to Ti(III) ions (species I′ and I″) and $Ti(O_2^{-\cdot})$ radicals (species II) are indicated.

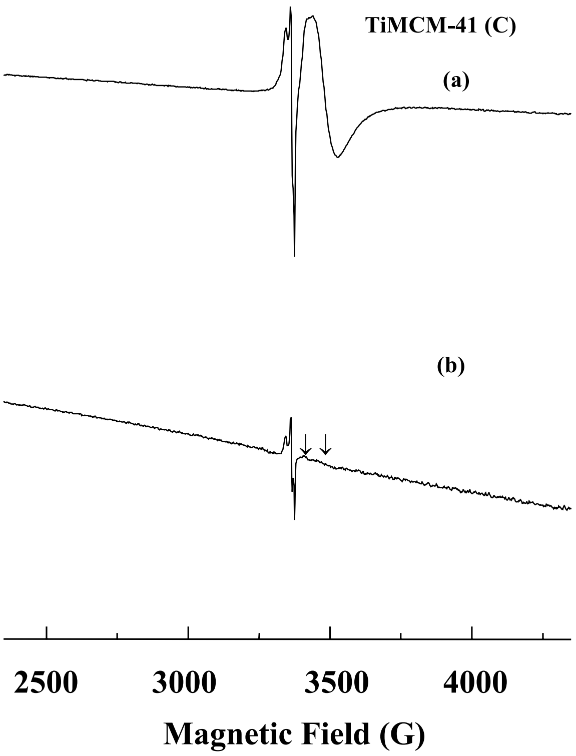

Fig. 4. ESR spectra (at 77 K) of dry hydrogen-reduced Ti-MCM-41(C): (a) before exposing to air and (b) after exposing to air.

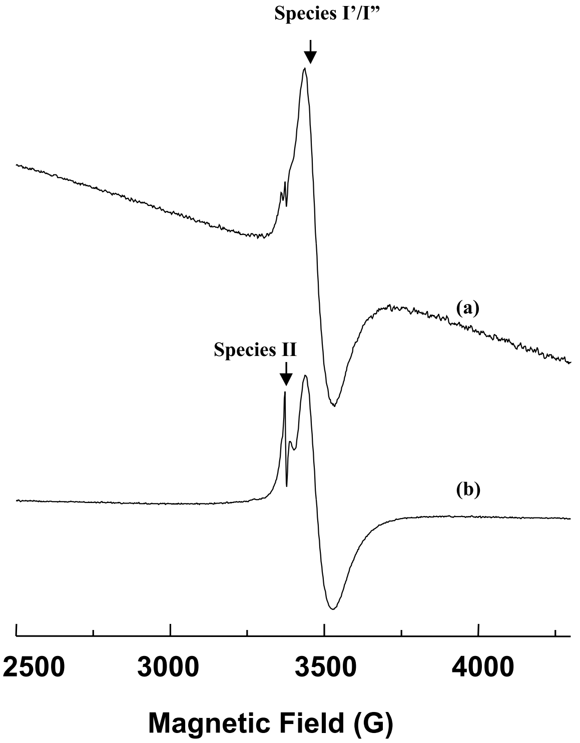

Fig. 5. ESR spectra (at 77 K) of Ti-MCM-41 after reduction with $LiAlH_4$: (a) sample C and (b) sample B. Signals due to Ti(III) ions (species I′ and I″) and Ti(O_2^-) radicals (species II) are marked.

Reactions with $LiAlH_4$ at 298 K also yielded the Ti(III) species (Fig. 5). The corresponding spectra for Zr-MCM-41 were reported earlier [30]. The ESR signal intensity reveals that the extent of reduction is higher with $LiAlH_4$ than with dry hydrogen.

Reactions with aqueous H_2O_2 and TBHP yielded the metal superoxide species. The spectra of Ti-MCM-41 and Zr-MCM-41 reacted with H_2O_2 are shown in Fig. 6. Metal superoxide species have been proposed as intermediates in catalytic oxidation reactions by titanosilicates [1,2,33,34]. It is interesting to note from the ESR studies (Fig. 4) that this intermediate metal superoxide species can also be generated by reduction with dry hydrogen/$LiAlH_4$ followed by re-oxidation with aerial oxygen.

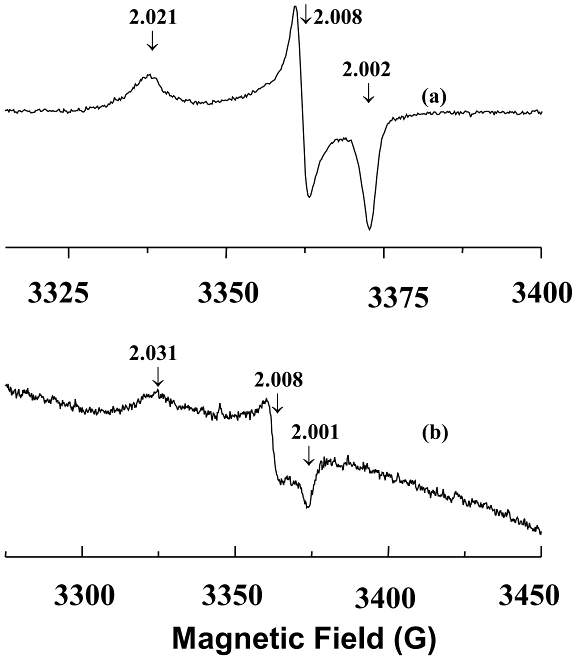

Fig. 6. ESR spectra at 77 K of the metal superoxide radicals generated by reacting (a) Ti-MCM-41(C) and (b) Zr-MCM-41(D) with aqueous H_2O_2.

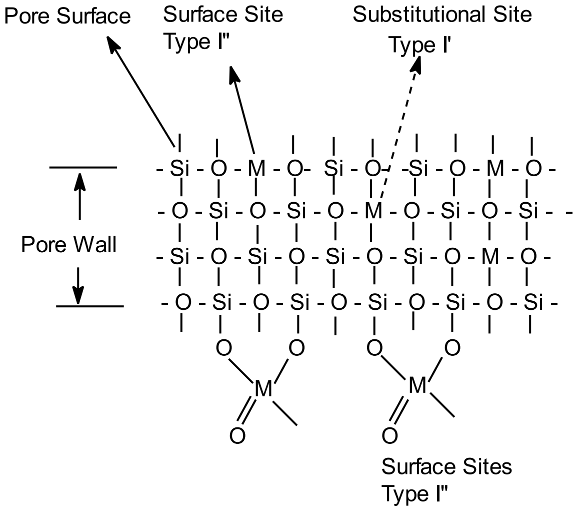

Scheme 1. Locations of Ti and Zr ions in (M)-MCM-41.

Spectral simulations reveal the presence of two types of metal ion species (I′ and I″). A generalized diagram showing the locations of different species is shown in Scheme 1. Species I′ is characterized by a rhombic *g* tensor and corresponds to the ions

Table 2
ESR spin Hamiltonian parameters of Ti-MCM-41 and Zr-MCM-41

Sample	Treatment	g_x	g_y	g_z	$c_{\parallel}/\Delta \times 10^{-5}$	$c_{\perp}/\Delta \times 10^{-5}$	Assignment
Ti-MCM-41	Reaction with dry H_2 at 873 K	1.938	1.974	1.894	8.734	14.940	Ti(III); species I′
		1.958	1.958	1.906	7.766	14.290	Ti(III); species I″
	Reaction with dry H_2 at 873 K and reoxidation with air	2.002	2.008	2.021	–	–	$Ti(O_2^{-\cdot})$; species II
	Reaction with H_2O_2	2.003	2.009	2.024	–	–	$Ti(O_2^{-\cdot})$; species II
Zr-MCM-41	Reaction with dry H_2 at 873 K	1.943	1.970	1.876	3.158	4.630	Zr(III); species I′
		1.961	1.961	1.899	2.583	4.130	Zr(III); species I″
	Reaction with dry H_2 at 873 K and reoxidation with air	2.001	2.008	2.031	–	–	$Zr(O_2^{-\cdot})$; species II
	Reaction with H_2O_2	2.002	2.009	2.032	–	–	$Zr(O_2^{-\cdot})$; species II

located inside the pore walls. Species I″, on the contrary is characterized by an axial g tensor and corresponds to the ions located at the surface of the pores. The spin Hamiltonian parameters of species I′ and I″ along with those of Ti(IV)-superoxide radicals ($TiO_2^{-\cdot}$) (species II; not shown in Scheme 1) are listed in Table 2. The data for Zr species [30] are included for the sake of completeness. Although both Ti(III) and Zr(III) have a single unpaired electron ($S = 1/2$) in the d-orbitals, the g-values of these are markedly different, especially in the g_z parameter. A difference in the g_z parameter of the superoxide species is also noticed. This difference is related to the crystal field splitting and the covalency of metal–oxygen bond. The g values of M(III) ions, with $g_z < g_x/g_y < 2.0023$, correspond to a distorted tetrahedral geometry, with a $d_{x^2-y^2}$ ground state. The expressions for the g-values in the case of an axial symmetry are as follows:

$$g_{\perp} = 2.0023 - (8c_{\perp}\lambda/\Delta)$$

$$g_{\parallel} = 2.0023 - (2c_{\parallel}\lambda/\Delta)$$

where λ is the spin–orbit coupling constant. Its value for Ti(III) is 155 cm^{-1} and for Zr(III) is 500 cm^{-1}; Δ is crystal field splitting; $g_{\parallel}$ corresponds to g_z and $g_{\perp}$ is approximated to $(g_x + g_y)/2$. The coefficients $c_{\perp}$ and $c_{\parallel}$ are related to metal–oxygen covalency parameters. The parameters $c_{\perp}/\Delta$ and $c_{\parallel}/\Delta$ for species I′ and I″ of Ti-MCM-41 and Zr-MCM-41 were estimated (Table 2) by substituting the experimental g values in the above expressions. These values are smaller for Zr-MCM-41 than for Ti-MCM-41. However, one expects smaller values for Ti-MCM-41 than for Zr-MCM-41, as the covalency of Ti–O is more than Zr–O bond. The reverse trend for $c_{\perp}/\Delta$ and $c_{\parallel}/\Delta$ is therefore due to a difference in the crystal field parameter (Δ) for Ti-MCM-41 and Zr-MCM-41 samples. The Δ value for Zr-MCM-41 is larger than that for Ti-MCM-41. This is perhaps due to a higher distortion in the case of the zirconium samples due to a larger difference in the covalent radii of Zr(IV) and Si(IV) than of Ti(IV) and Si(IV).

3.2. Catalytic activity studies

3.2.1. Hydroxylation of 1-naphthol

Both Ti-MCM-41 and Zr-MCM-41 were active in the hydroxylation of 1-naphthol with aqueous H_2O_2 as oxidant. The results of the hydroxylation reactions are presented in Table 3. For comparison the reactions were also carried out over the impregnated and all-silica MCM-41 samples. The impregnated samples showed very low activity (~1 mol% conversion) while Si-MCM-41 exhibited no activity. Also, no activity was observed in the absence of the Ti- or Zr-MCM-41 catalysts. These results indicate that Ti and Zr ions are responsible

Table 3
Catalytic activities of Ti-MCM-41 and Zr-MCM-41 in the hydroxylation of 1-naphthol with H_2O_2[a]

Sample	Convesion (mol%)	TOF (h^{-1})	Product distribution (mol%)			H_2O_2 selectivity (mol%)[b]
			1,4-naphtho-quinone	1,4-dihydroxy-naphthalene	1,2-dihydroxy-naphthalene	
Ti-MCM-41(A)	14.1	0.8	100	–	–	42.3
Ti-MCM-41(B)	21.5	0.7	100	–	–	64.5
Ti-MCM-41(C)	29.7	0.5	97	0.3	2.7	87.8
Zr-MCM-41(A)	10.2	0.9	95.4	1.9	2.7	29.9
Zr-MCM-41(B)	14.2	0.7	94.3	2.6	3.1	41.4
Zr-MCM-41(D)	17.8	0.4	92.6	3.7	3.7	51.4

[a] Reaction conditions: catalyst = 0.1 g, 1-naphthol = 0.5 g, 1-naphthol/H_2O_2 = 1.5 (mol), solvent = CH_3CN (10 g); temperature = 353 K, duration = 24 h. TOF = number of moles of 1-naphthol converted per mole of Ti or Zr per hour.

[b] H_2O_2 selectivity (mol%) = number of moles of H_2O_2 utilized in product formation/number of moles of H_2O_2 fed) × 100; all H_2O_2 fed was consumed at 24 h.

for the catalytic activity. The reaction was highly selective for 1,4-naphthaquinone (100 mol% selectivity with Ti-MCM-41 and 90.5–95.4 mol% with Zr-MCM-41); 1,4-dihydroxynaphthalene and 1,2-dihydroxynaphthalene were minor products of the hydroxylation reaction (Scheme 2). Distinct variations in the conversion and turnover frequency (TOF) with varying metal contents were observed. With increasing metal content the conversion of 1-naphthol increased, while the TOF decreased. The selectivity for 1,4-naphthaquinone also decreased with increasing metal content.

3.2.2. Epoxidation of norbornylene

Both Ti-MCM-41 and Zr-MCM-41 were active in the epoxidation of norbornylene with TBHP (Table 4). As in the case of hydroxylation reactions, impregnated samples showed very low conversions (1 mol%) in the epoxidation reaction. Si-MCM-41 was not active. The reaction did not proceed in the absence of the Ti- or Zr-MCM-41 catalysts. Oxidation of norbornylene over Ti-MCM-41 and Zr-MCM-41 yielded exo- and endo-epoxides which opened up further during the reaction to give the corresponding diols. The various products of the epoxidation reaction are shown in Scheme 2. Zr-MCM-41 samples showed conversions in the range of 31.8–46.5 mol% while the conversion on Ti-MCM-41 samples was in the range 38.4–54.1 mol% (Table 4). The reaction was more selective for the exo- than for the endo-epoxide. The conversion, in general, increased with

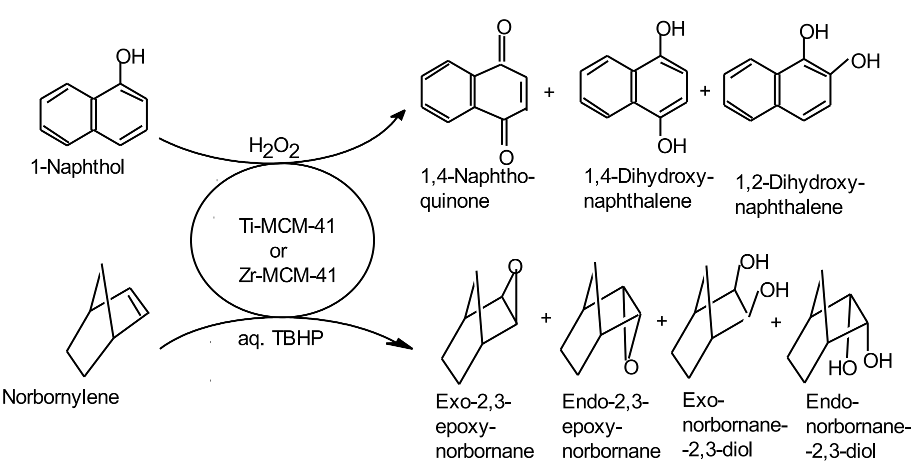

Scheme 2. Oxidation of 1-naphthol and norbornylene.

Table 4
Catalytic activities of Ti-MCM-41 and Zr-MCM-41 in the epoxidation of norbornylene with TBHP[a]

Sample	Conversion (mol%)	TOF (h^{-1})	Product distribution (mol%)			
			Endo-2, 3-epoxy-norbornane	Exo-2, 3-epoxy-norbornane	Diol[b]	Others
Ti-MCM-41(A)	38.4	3.3	3.5	87.5	7.5	1.4
Ti-MCM-41(B)	42.2	2.0	2.9	84.1	9.6	3.4
Ti-MCM-41(C)	54.1	1.4	2.4	60.6	34.1	2.9
Zr-MCM-41(A)	31.8	4.2	3.2	78.9	12.6	5.3
Zr-MCM-41(B)	37.9	2.9	3.9	80.4	13.2	2.5
Zr-MCM-41(C)	46.5	2.5	4.2	84.7	9.8	1.3
Zr-MCM-41(D)	41.7	1.4	9.6	64.8	19.8	5.8

[a] Reaction conditions: catalyst = 0.1 g, norbornene = 0.5 g, norbornene/H_2O_2 = 1.5 (mol), solvent = CH_3CN (10 g); temperature = 343 K, duration = 24 h. TOF = number of moles of norbornylene converted per mole of Ti or Zr per hour.

[b] Diol = endo-2, 3-norbornanediol + exo-2, 3-norbornanediol.

increasing metal content, while the variation of TOF showed a reverse trend. The selectivity for the epoxide also decreased (from 87% to 60% with TiMCM-41 and 84% to 65% with ZrMCM-41) with increasing metal content, while the total alcohol content increased.

3.3. Redox behavior and catalytic activity correlations

The position of the charge transfer band in the DRUV–Vis spectra at 220 nm for Ti-MCM-41 and 208 nm for Zr-MCM-41, the increase in the pore diameter and pore volume with increasing metal content, the characteristic Si–O–(M) band in the FT-IR spectra and ESR spectral features together reveal that Ti and Zr ions are substituted in place of Si in the MCM-41 structure. Both the Ti and Zr ions can be reduced from the +4 to the +3 oxidation state. The normalized ESR intensity of the reduced species, obtained by double integration of the signals, is higher for Ti-MCM-41 by an order of magnitude than that for Zr-MCM-41 and indicates that Ti is easier to reduce than Zr. ESR spectra of the reduced samples reveal two types of metal ions, viz., species I' and I'' corresponding to the ions located inside the pore walls and to those at the pore surface, respectively. Species I'' are more abundant than species I' in samples with high Zr loading. However, in Ti-MCM-41, incorporation of Ti into the pore walls (species I') is particularly high. Because of the overlap of signals, quantification of different species using ESR spectroscopy was not possible. Although the charge transfer band in the DRUV–Vis spectra reveals a dispersion of metal ions, a small amount of metal oxide patches or nanoparticles cannot be excluded in samples with higher metal contents. The Ti-MCM-41 and Zr-MCM-41 samples show similar catalytic oxidation activity (conversion and TOF) as revealed from Tables 3 and 4. The low activity of the impregnated samples indicates that monoatomic dispersion and substitution of metal ions in the silicate framework are the causes for the activity. From the redox behavior and the nature of M–O bonding one would expect a higher activity for the Ti than for the Zr-silicates. However, the Ti and Zr samples exhibit similar activities. It is interesting to note that Gontier and Tuel [35] have also made a similar observation for titanium- and zirconium-containing mesoporous silicas (Ti-MS and Zr-MS) in oxidation reactions. Ti is located mostly in the pore walls leaving a small number of accessible sites at the pore surface for reactions with large substrates. The similarities in activity (TOF; Tables 3 and 4) of the Ti and Zr catalysts, inspite of the lower availability of the Ti sites for the reactions, suggests an intrinsically larger activity of the Ti ions (compared to Zr) as a result, perhaps, of its easier redox transformation.

4. Conclusions

ESR studies on reduced samples of Ti- and Zr-MCM-41 reveal the presence of metal ions located inside the pore walls (species I′) and at the surface of the pores (species I″). The reduced ions, especially species I″ are highly reactive towards aerial oxygen and form $M(O_2^{-\cdot})$ species, an active intermediate invoked in the oxidation reactions involving metallosilicates. The Ti samples are easier to reduce than the Zr samples. Both Ti- and Zr-MCM-41 are catalytically active in hydroxylation/oxidation reactions in the presence of H_2O_2/TBHP.

Acknowledgements

KC and RB acknowledge CSIR, New Delhi, for financial support in the form of senior research fellowships.

References

[1] N. Vayssilov, Catal. Rev.-Sci. Engng. 39 (1997) 209.
[2] B. Notari, Adv. Catal. 41 (1996) 253.
[3] C.T. Kresge, M.E. Leonowicz, W.J. Roth, J.C. Vartuli, J.S. Beck, Nature 359 (1992) 710.
[4] J.S. Beck, J.C. Vartuli, W.J. Roth, M.E. Leonowicz, C.T. Kresge, K.D. Schmit, C.T.-W. Chu, D.H. Olson, E.W. Sheppard, S.B. McCullen, J.B. Higgins, J.L. Schlenker, J. Am. Chem. Soc. 114 (1992) 10834.
[5] D. Zhao, J. Feng, Q. Huo, N. Melosh, G.H. Fredrickson, B.F. Chmelka, G.D. Stucky, Science 279 (1998) 548.
[6] A. Corma, Chem. Rev. 97 (1997) 2373.
[7] Y. Ma, W. Tong, H. Zhou, S.L. Suib, Micropor. Mesopor. Mater. 37 (2000) 243.
[8] D. Zhao, Q. Huo, J. Feng, B.F. Chmelka, G.D. Stucky, J. Am. Chem. Soc. 120 (1998) 6024.
[9] L. Luan, C.F. Cheng, W. Zhou, J. Klinowski, J. Phys. Chem. 99 (1995) 1018.
[10] R. Ryoo, J.H. Kim, J. Chem. Soc. Chem. Commun. (1995) 711.
[11] R. Mokaya, W. Jones, J. Chem. Soc. Chem. Commun. (1996) 983.
[12] R. Schmidt, D. Akporiaye, M. Stöcker, O.H. Ellestad, J. Chem. Soc. Chem. Commun. (1994) 1493.
[13] P.T. Tanev, M. Chibwe, T.J. Pinnavaia, Nature 368 (1994) 321.
[14] A. Corma, M.T. Navarro, J. Perez-Pariente, J. Chem. Soc. Chem. Commun. (1994) 147.
[15] Z.Y. Yuan, S.O. Liu, T.H. Chen, J.Z. Wang, H.X. Li, J. Chem. Soc. Chem. Commun. (1995) 973.
[16] D. Zhao, D. Goldfarb, J. Chem. Soc. Chem. Commun. (1995) 875.
[17] K.M. Reddy, I. Moudrakovski, A. Sayari, J. Chem. Soc. Chem. Commun. (1994) 1059.
[18] M. Morey, A. Davidson, G. Stucky, Micropor. Mater. 6 (1996) 99.
[19] Y.X. Zhi, A. Tuel, Y. Ben Taarit, C. Naccache, Zeolites 12 (1992) 138.
[20] C.F. Cheng, J. Klinowski, J. Chem. Soc. Faraday Trans. 92 (1996) 289.
[21] J.-S. Yu, J.Y. Kim, L. Kevan, Micropor. Mesopor. Mater. 40 (2000) 135.
[22] A. Brait, M.E. Davis, Appl. Catal. A: General 204 (2000) 117.
[23] I. Diaz, F. Mohino, J. Perez-Pariente, E. Sastre, Appl. Catal. A: General 205 (2001) 19.
[24] X.X. Wang, F. Lefebvre, J. Patarin, J.-M. Basset, Micropor. Mesopor. Mater. 42 (2001) 269.
[25] Z. Zhu, M. Hartmann, E.M. Macs, R.S. Czernuszewicz, L. Kevan, J. Phys. Chem. B 104 (2000) 4690.
[26] A.M. Prakash, H.M. Sung-Suh, L. Kevan, J. Phys. Chem. B 102 (1998) 857.
[27] Z. Luan, L. Kevan, J. Phys. Chem. B 101 (1997) 2020.
[28] R.M. Krishna, A.M. Prakash, L. Kevan, J. Phys. Chem. B 104 (2000) 1796.
[29] K. Chaudhari, T.K. Das, P.R. Rajmohanan, K. Lazar, S. Sivasanker, A.J. Chandwadkar, J. Catal. 183 (1999) 281.
[30] K. Chaudhari, R. Bal, T.K. Das, A. Chandwadkar, D. Srinivas, S. Sivasanker, J. Phys. Chem. B 104 (2000) 11066.
[31] E.P. Barret, L.G. Joyner, P.P. Halenda, J. Am. Chem. Soc. 73 (1951) 373.
[32] M. Anpo, M. Che, B. Fubini, E. Farrone, E. Giamello, M.C. Paganini, Top. Catal. 8 (1999) 189.
[33] R.F. Parton, D.R.C. Huybrechts, Ph. Buskens, P.A. Jacobs, in: G. Öhlmann, H. Pfeifer, R. Fricke (Eds.), Catalysis and Adsorption by Zeolites, Studies in Surface Science and Catalysis, vol. 65, Elsevier, Amsterdam, 1991, p. 47.
[34] S. Biz, M.L. Occelli, Catal. Rev.-Sci. Engng. 40 (1998) 329.
[35] S. Gontier, A. Tuel, Appl. Catal. A: General 143 (1996) 125.